



Centrum voor Wiskunde en Informatica

REPORTRAPPORT

Modeling of Air Sparging in a Layered Soil: Numerical and Analytical
Approximations

M.I.J. van Dijke, S.E.A.T.M. van der Zee

Modelling, Analysis and Simulation (MAS)

MAS-R9729 October 31, 1997

Report MAS-R9729
ISSN 1386-3703

CWI
P.O. Box 94079
1090 GB Amsterdam
The Netherlands

CWI is the National Research Institute for Mathematics and Computer Science. CWI is part of the Stichting Mathematisch Centrum (SMC), the Dutch foundation for promotion of mathematics and computer science and their applications.

SMC is sponsored by the Netherlands Organization for Scientific Research (NWO). CWI is a member of ERCIM, the European Research Consortium for Informatics and Mathematics.

Copyright © Stichting Mathematisch Centrum
P.O. Box 94079, 1090 GB Amsterdam (NL)
Kruislaan 413, 1098 SJ Amsterdam (NL)
Telephone +31 20 592 9333
Telefax +31 20 592 4199

Modeling of Air Sparging in a Layered Soil: Numerical and Analytical Approximations

M.I.J. van Dijke

CWI

P.O. Box 94079, 1090 GB Amsterdam, The Netherlands

S.E.A.T.M. van der Zee

Department of Soil Science and Plant Nutrition, Wageningen Agricultural University

P.O. Box 8005, 6700 EC Wageningen, The Netherlands

ABSTRACT

Air sparging in an aquifer below a less permeable horizontal layer is modeled using a two-phase flow approach. Supported by numerical simulations we show that a steady state situation is reached. For an analysis of the steady state we distinguish three different flow regimes, which occur between the well screen and the unsaturated zone. Just below the interface, that separates the high and the low permeable layers, a regime with almost hydrostatic capillary pressures develops. We use this observation to derive an ordinary differential equation for the pressure at the interface, which leads to an approximation of the air flow pattern just below and within the low permeable layer. The approximation provides an estimate for the radius of influence as a function of the physical parameters. The agreement between the analytical approximation and the numerical steady state results is almost perfect when heterogeneity is increased. With a few modifications the analysis applies also to a DNAPL spill above a less permeable layer. Comparison with an illustrative numerical simulation shows that the analytical approximation provides a good estimate of the radial spreading of the DNAPL flow on top of and within the low permeable layer.

1991 Mathematics Subject Classification: 35K57, 65M60, 76S05, 76T05

Keywords and Phrases: two-phase flow, air sparging, soil layering, vertical equilibrium, analytical approximation, numerical simulations

Note: Work carried out under project MAS1.3 "Partial Differential Equations in Porous Media Research".

1. INTRODUCTION

A method for remediating an aquifer which is contaminated by organic liquids (solvents, gasoline) trapped in the saturated zone, is to inject air or oxygen into the aquifer. Injection of air into the saturated zone, known as air sparging, may enhance microbial degradation and volatilization.

Experimental studies on air sparging on both field [*Johnson et al.*, 1993; *Lundegard and LaBrecque*, 1995; *Marley et al.*, 1992] and laboratory [*Ji et al.*, 1993; *Wehrle*, 1990] scales intended to determine the region in the saturated zone where air is present (radius of influence). These studies revealed that variations in soil texture strongly affect the air flow. Air sparging is only possible in relatively coarse-grained soils [*Johnson et al.*, 1993] and in most cases air flow appears to occur in small continuous channels.

The assumption of flow continuity allows modeling of air sparging as a multi-phase flow process [*McCray and Falta*, 1996; *Mohtar et al.*, 1994; *Van Dijke et al.*, 1995]. Besides flow continuity, air-phase compressibility may be a complicating factor in modeling air sparging. A previous paper [*Van Dijke et al.*, 1995], that was supported by a field study [*Lundegard and LaBrecque.*, 1995], concluded that in the steady state situation in which continuous channels to the vadose zone exist, compressibility is likely to play a minor role.

Considering air and water as two immiscible incompressible continuous phases, the effect of soil, fluid and well parameters on the radius of influence of a single injection well in a homogeneous medium was analyzed [Van Dijke *et al.*, 1995]. In many situations, however, aquifers contain less permeable regions, which may control the main direction of air flow. Several numerical studies [McCray and Falta, 1996; Unger *et al.*, 1995] have demonstrated the effect of heterogeneities. In this paper we model air sparging below a less permeable horizontal layer with large lateral extension. We assume that the different layers have similar structure but different mean pore size, i.e. the similar media assumption [Leverett, 1941; Miller, 1980]. We aim at investigating the air flow through layered soils, in particular the quantitative effect of the degree of heterogeneity and the position of the interface, that separates the layers, on the resulting radius of influence.

In Section 2 we present the transient model: the basic equations with their saturation dependent relative permeability and capillary pressure functions and the geometry of the domain including the two different layers. To accommodate analysis of the steady state situation, we reformulate the problem in dimensionless form and identify the governing dimensionless numbers. Thus, we present similar equations with different parameters for the two subdomains, which are linked by continuity of capillary pressure and of the vertical air velocity component at the interface.

In Section 3 we analyze the steady state situation that occurs when air flow from the injection well to the vadose zone has been established. Emphasis is given to the region just below the interface, where air mainly spreads horizontally. We assume that flow in this region is ruled by vertical equilibrium, despite a small vertical air velocity component across the interface. An ordinary differential equation for the capillary pressure at the interface governs the radial extension of air below the interface.

In Section 4 we present the results of numerical simulations that are based on the transient model, which show that indeed a steady state situation is approached. In terms of capillary pressure the numerical solutions are compared to the analytical approximation. On the basis of our analytical approximation, we carried out a sensitivity analysis of the effect of the dimensionless numbers, especially the measure of the heterogeneity, on the saturation profile at the interface.

Our analysis relates to a study on flow of dense nonaqueous phase liquid (DNAPL) on top of a low permeable layer of finite horizontal extension, which provides conditions for DNAPL infiltration into the layer in terms of the contrast in entry pressures [De Neef and Molenaar, 1997]. Therefore, we show in Section 5 that with a few modifications, the present study may also reveal how DNAPL leaks through a low permeable layer of large horizontal extension. An illustrative simulation shows the analogy between the sparging and the DNAPL flow processes.

2. MODEL

According to [Van Dijke *et al.*, 1995] we use for both air (a) and water (w) Darcy's Law

$$\vec{U}_j = -\frac{k k_{rj}}{\mu_j} \nabla (P_j + \rho_j g Z), \quad j = w, a \quad (2.1)$$

and the mass balance equations

$$\phi \frac{\partial S_j}{\partial t} + \nabla \cdot \vec{U}_j = 0 \quad j = w, a, \quad (2.2)$$

where k denotes soil intrinsic permeability, ϕ soil porosity, S_j effective fluid saturation, \vec{U}_j fluid Darcy velocity, k_{rj} fluid relative permeability, μ_j fluid viscosity, P_j fluid pressure, ρ_j fluid density and g gravity. We assume that both fluids are incompressible and that the soil is isotropic, but consists of two layers.

The constitutive relations $S_w + S_a = 1$, the capillary pressure $P_c = P_a - P_w$, $S_j = S_j(P_c)$ and $k_{rj} = k_{rj}(S_j)$ complete the set of equations (2.1) and (2.2). The dependence of capillary pressure and

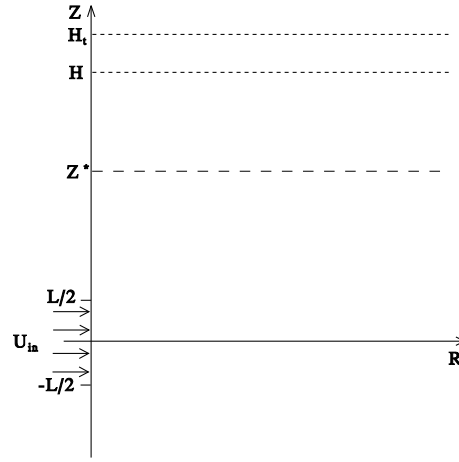


Figure 1: Schematic of the domain for air sparging. Air is injected at the well radius $R = E$ between $Z = -L/2$ and $Z = L/2$ with constant velocity U_{in} . H_t denotes the soil surface, H the initial position of the water table and Z^* the position of the interface between the low (top) and high permeable (bottom) layers.

relative permeability on the saturations is given by the expressions [Parker *et al.*, 1987]

$$P_c(S_a) = \frac{\rho_w g}{\alpha} ((1 - S_a)^{-\frac{1}{m}} - 1)^{1-m} \quad (2.3)$$

$$k_{rw}(S_w) = S_w^{\frac{1}{2}} (1 - (1 - S_w^{\frac{1}{m}})^m)^2 \quad (2.4)$$

$$k_{ra}(S_a) = S_a^{\frac{1}{2}} (1 - (1 - S_a)^{\frac{1}{m}})^{2m}, \quad (2.5)$$

where $0 < m < 1$ is a given constant. The parameter $\alpha > 0$ differs for each layer and reflects the air-water capillary forces in a soil.

Equations (2.1) and (2.2) are solved in the two-dimensional axially symmetric domain of Figure 1 for time $T > 0$. The level $Z = H$ corresponds to the initial position of the water table. Hence, the water pressure along the top boundary of the domain, the soil surface $Z = H_t$, is $P_w = \rho_w g (H - H_t)$, and the air pressure equals $P_a = 0$. For $T > 0$, air is injected with velocity U_{in} into this domain through a vertical well screen with radius $E > 0$, located between $Z = \pm L/2$. This yields a total injection rate $Q = 2\pi ELU_{in}$. The remaining part of the vertical line $R = E$ that represents the well casing, is impermeable.

We consider two subdomains, separated by an interface at depth $Z = Z^*$, where

$$k = \begin{cases} k^- & \text{for } Z < Z^* \\ k^+ & \text{for } Z > Z^* \end{cases} \quad \text{and} \quad \alpha = \begin{cases} \alpha^- & \text{for } Z < Z^* \\ \alpha^+ & \text{for } Z > Z^* \end{cases}. \quad (2.6)$$

We assume that the two layers have similar structure, reflected by a single m -value for the entire domain, but that they have different mean pore size. Hence, in agreement with the scaling theory of similar media [Leverett, 1941; Miller, 1980] we take $k^+ = \gamma^2 k^-$ and $\alpha^+ = \gamma \alpha^-$, with constant k^- and α^- and heterogeneity factor $0 < \gamma < 1$. At the interface $Z = Z^*$, we have continuity of capillary pressure P_c and of the vertical components of the Darcy velocities $U_{j,z}$.

With numerical simulations, which are described in Section 4, we show that flow approaches a steady state. At steady state the water pressure is approximately hydrostatic [McCray and Falta, 1996; Van Dijke *et al.*, 1995] and the mass balance

$$\nabla \cdot \vec{U}_a = 0, \quad (2.7)$$

describes air flow, with

$$\vec{U}_a = -\frac{k k_{ra}}{\mu_a} \nabla (P_c - \Delta\rho g Z), \quad (2.8)$$

where $\Delta\rho = \rho_w - \rho_a$.

We introduce the dimensionless variables

$$r = \frac{R}{H}, \quad z = \frac{Z}{H}, \quad \vec{u}_a = \frac{\vec{U}_a}{U_{in}}, \quad p_c = \frac{\alpha^- P_c}{\rho_w g}, \quad (2.9)$$

where H , the depth of the well screen center below the water table, is chosen as a characteristic length. Furthermore, we define the dimensionless constants

$$\varepsilon = \frac{E}{H}, \quad z^* = \frac{Z^*}{H}, \quad h_t = \frac{H_t}{H} \quad (2.10)$$

and

$$N_g = \frac{k^- \Delta\rho g}{\mu_a U_{in}}, \quad N_c = \frac{k^- \rho_w g}{\mu_a U_{in} H \alpha^-}, \quad A = \frac{Q}{U_{in} H^2} \quad (2.11)$$

which are the gravity number, the capillary number and the dimensionless well screen surface respectively. The resulting equations are

$$\nabla \cdot \vec{u}_a = 0, \quad (2.12)$$

with

$$\vec{u}_a = \begin{cases} -N_c k_{ra} \nabla p_c + N_g k_{ra} \vec{e}_z & \text{for } z < z^* \\ -\gamma N_c k_{ra} \nabla p_c + \gamma^2 N_g k_{ra} \vec{e}_z & \text{for } z > z^*, \end{cases} \quad (2.13)$$

where \vec{e}_z is the unit vector in the vertical direction. The capillary pressure function has transformed into

$$p_c(S_a) = \begin{cases} \bar{p}_c(S_a) & \text{for } z < z^* \\ \frac{1}{\gamma} \bar{p}_c(S_a) & \text{for } z > z^*, \end{cases} \quad \text{with } \bar{p}_c(S_a) = ((1 - S_a)^{-\frac{1}{m}} - 1)^{1-m}. \quad (2.14)$$

As shown in [Van Dijke *et al.*, 1995] the combined dimensionless numbers

$$N_1 = \frac{N_g}{N_c} = \frac{\Delta\rho}{\rho_w} \quad \text{and} \quad N_2 = \frac{A}{\pi N_g} = \frac{Q \mu_a}{\pi k^- \Delta\rho g H^2} \quad (2.15)$$

and the exponent m determine the steady state flow problems. The number N_2 follows from the total flow rate

$$2\pi \int_0^\infty r u_{a,z} dr = A, \quad (2.16)$$

Furthermore, z^* and γ characterize the position and the degree of heterogeneity.

3. STEADY STATE FLOW ANALYSIS

To analyze the steady state situation we distinguish three regions which have different air flow regimes as shown in Figure 2. Provided that the distance between the well screen and the interface is large enough, we assume that upwards from the well screen a region (*I*) exists where buoyancy-induced forces dominate the vertical velocity component. In view of a study on DNAPL infiltration above

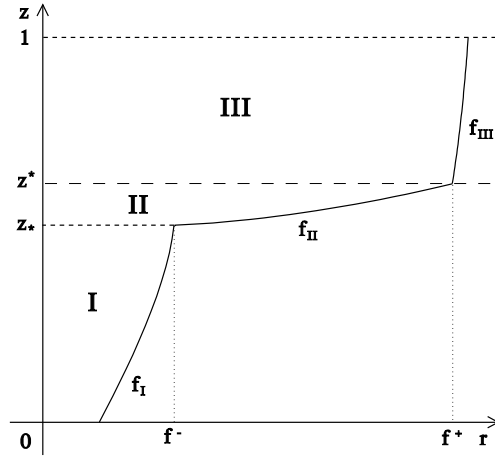


Figure 2: Air-invaded regions in the dimensionless domain with different steady state flow regimes. In regions *I* and *III* vertical flow is buoyancy-dominated. In region *II* the gravity and capillary forces in vertical direction are of equal magnitude and air spreads mainly in radial direction. The regions are radially enclosed by the free boundaries f_I , f_{II} and f_{III} respectively. The level $z = 0$ denotes the position of the well screen, the level $z = z_*$ separates regions *I* and *II*, the level $z = z^*$ denotes the interface between the layers and the level $z = 1$ the initial position of the water table.

a low permeable layer [De Neef and Molenaar, 1997] and supported by our numerical simulations, we expect that just below the interface that separates the low and the high permeable subdomains, a region (*II*) exists where the radial spreading of the air flow is much larger than in the buoyancy-dominated region, whereas in the vertical direction capillary and gravity forces are of equal magnitude. We assume that above the interface and below the water table (region *III*) the vertical flow is also buoyancy-driven. The three regions are enclosed outward by the free boundaries $r = f_I(z)$, $r = f_{II}(z)$ and $r = f_{III}(z)$ respectively.

In region *I* saturations are significantly smaller than one, which allows approximation of the relations between saturation, relative permeability and (reduced) capillary pressure by simple power law functions [Van Dijke et al., 1995]. The relations for the saturation and the (reduced) capillary pressure in terms of the relative permeability are

$$S_a(k_{ra}) \sim n_S k_{ra}^{p_S} \quad \text{and} \quad \bar{p}_c(k_{ra}) \sim \frac{n_D}{p_D} k_{ra}^{p_D}, \quad (3.1)$$

where

$$n_S = m \frac{4m}{4m+1}, \quad p_S = \frac{2}{4m+1}, \quad n_D = \frac{2(1-m)}{4m+1} m \frac{m-1}{4m+1}, \quad p_D = \frac{2(1-m)}{4m+1}. \quad (3.2)$$

Considering the well as a point source and neglecting the well screen diameter, the air flow is described by a similarity solution, the Barenblatt-Pattle point source solution [Barenblatt, 1952; Pattle, 1959; Van Dijke et al., 1995], that in terms of capillary pressure is given by

$$p_c(r, z) = \begin{cases} \left(\frac{p_D + 1}{p_D} \frac{N_2}{f^2(z)} \right)^{p_D} \left(1 - \frac{r^2}{f^2(z)} \right) & \text{for } 0 \leq r \leq f(z), \quad z > 0 \\ 0 & \text{for } r > f(z), \quad z > 0. \end{cases} \quad (3.3)$$

The free boundary f separating the regions with and without air is given by

$$f(z) = f_0 z^{\frac{1}{2(p_D+1)}} \quad \text{for } z \geq 0 \quad (3.4)$$

with

$$f_0 = \left(\frac{4n_D}{N_1} N_2^{p_D} \right)^{\frac{1}{2(p_D+1)}} \left(\frac{p_D+1}{p_D} \right)^{\frac{1}{2}}. \quad (3.5)$$

This approximation is valid for (r, z) in region *I*, where $f_I(z) = f(z)$.

To develop an approximate solution for region *II*, we consider the continuity conditions at the interface. Continuity of the vertical component of the velocity yields with (2.13)

$$\lim_{z \uparrow z^*} -N_c k_{ra} \frac{\partial p_c}{\partial z} + N_g k_{ra} \sim \lim_{z \downarrow z^*} \gamma^2 N_g k_{ra} \quad (3.6)$$

assuming that above the interface buoyancy is dominant. Continuity of pressure yields with (2.14)

$$\lim_{z \downarrow z^*} \bar{p}_c = \gamma \lim_{z \uparrow z^*} \bar{p}_c, \quad (3.7)$$

which shows for $\gamma < 1$ that saturations and relative permeabilities above the interface are smaller than below, i.e.

$$\lim_{z \downarrow z^*} k_{ra} < \lim_{z \uparrow z^*} k_{ra}. \quad (3.8)$$

Hence, we may neglect the righthandside of relation (3.6), and we obtain for the pressure gradient just below the interface

$$\frac{\partial p_c}{\partial z} \sim \frac{N_g}{N_c}. \quad (3.9)$$

Equation (3.9) is the vertical equilibrium assumption, which controls flow in region *II*. Neglecting for convenience the transition zone between the buoyancy-dominated and the vertical equilibrium regime, regions *I* and *II* meet at some level $z = z_*$ ($0 < z_* < z^*$) as shown in Figure 2. Here, we define f^- as the radial position where f_I changes into f_{II} . Furthermore, f^+ indicates the radial position where f_{II} changes into f_{III} .

Especially if the contrast of material properties below and above the interface is large ($\gamma \ll 1$), we expect that $f^- \ll f^+$. Consequently, we assume that the buoyancy-dominated regime only slightly affects the vertical equilibrium regime. Hence, we analyze the flow in region *II* separately, thus neglecting continuity with region *I* at $z = z_*$, except that the total flow rate condition (2.16) is satisfied for every horizontal plane.

We vertically integrate in region *II* the hydrostatic pressure relation (3.9) till the interface, i.e.

$$p_c(r, z) = p(r) - \frac{N_g}{N_c} (z^* - z), \quad (3.10)$$

which shows that the capillary pressure at the interface $p(r) = p_c(r, z^*)$ also determines the capillary pressure elsewhere in the vertical equilibrium region. Furthermore, relation (3.10) specifies a boundary $z = z_f(r)$ for $\varepsilon \leq r \leq f^+$, where $p_c = 0$, i.e.

$$z_f(r) = z^* - \frac{N_c}{N_g} p(r). \quad (3.11)$$

We vertically integrate the mass balance equation (2.12) from z_f to z^* , which yields

$$\frac{\partial}{\partial r} \left(r \int_{z_f}^{z^*} u_{a,r} dz \right) + r u_{a,z}(r, z^*) = 0 \quad \text{for } \varepsilon < r < f^+. \quad (3.12)$$

To evaluate the integral, i.e. the effective horizontal flux, we derive from (3.10)

$$\frac{\partial p_c}{\partial r} = \frac{dp}{dr} \quad \text{and} \quad dz = \frac{N_c}{N_g} dp_c, \quad (3.13)$$

leading to

$$\int_{z_f}^{z^*} u_{a,r} dz = -N_c \int_{z_f}^{z^*} k_{ra} \frac{\partial p_c}{\partial r} dz = -\frac{N_c^2}{N_g} D(p) \frac{dp}{dr}. \quad (3.14)$$

The effective 'diffusion' coefficient is defined by $D = \int_0^p \kappa(\xi) d\xi$, with $\kappa(p_c) = k_{ra}(S_a(p_c))$, where ξ is a dummy variable for integration over the range of p_c values. By continuity the vertical velocity component $u_{a,z}(r, z^*)$ is given by the righthandside of relation (3.6). Using also continuity of capillary pressure (3.7), we obtain

$$-\frac{N_c^2}{N_g} \frac{d}{dr} (r D(p) \frac{dp}{dr}) + r \gamma^2 N_g \kappa(\gamma p) = 0. \quad (3.15)$$

Integration of equation (3.12) over r from ε to f^+ and application of the mass balance condition (2.16) at the interface yields the boundary condition

$$-2\pi \frac{N_c^2}{N_g} (r D(p) \frac{dp}{dr})|_{r=\varepsilon} = A \quad (3.16)$$

where we have used that the flux (3.14) vanishes at $r = f^+$. Hence, we must solve the boundary value problem

$$\begin{cases} \frac{d}{dr} (r D(p) \frac{dp}{dr}) - r \gamma^2 N_1^2 \kappa(\gamma p) = 0 & \text{for } \varepsilon < r < f^+ \\ -(r D(p) \frac{dp}{dr})|_{r=\varepsilon} = \frac{N_1^2 N_2}{2}, \quad p(f^+) = 0, \end{cases} \quad (3.17)$$

for $p(r)$, where we have used definitions (2.15) for N_1 and N_2 . In Appendix 1 we show that at $r = f^+$ the derivative $\frac{dp}{dr}(f^+)$ satisfies

$$\frac{dp}{dr}(f^+) = -\gamma^{1+\frac{1}{2pD}} N_1. \quad (3.18)$$

Hence, we solve problem (3.17) simultaneously for $p(r)$ and f^+ as described in Appendix 1.

Using the solution $p(r)$ in equation (3.11), we find $z = z_f(r)$. Intersection of $z = z_f(r)$ and $r = f(z)$ (3.4), yields the pair (f^-, z_*) . Hence, we approximate capillary pressure for $z < z_*$ (region *I*) by equation (3.3) and for $z_* < z < z^*$ (region *II*) by equation (3.10) and the solution $p(r)$ of system (A 3). The free boundary $r = f_{II}(z)$ along region *II* is given by $r = z_f^{-1}(z)$ for $z_* < z < z^*$.

Assuming that above the interface vertical flow is dominated by buoyancy and saturations are small, we may expect that the pressure distribution satisfies approximately the similarity profile (3.3). However, the radial extension of the air distribution is already so large at the interface, that upwards to the unsaturated zone the radial spreading according to this profile will be small. Moreover, numerical simulations show that in the vicinity of the water table the extension tends to decrease. Hence, we approximate for region *III*

$$p_c(r, z) = p_c(r, z^*) \quad \text{for } z > z^*, \quad (3.19)$$

with $f_{III}(z) = f^+$.

Table 1: Parameters and dimensionless numbers used in computations. Relative to the reference case (case 1), γ is varied for cases 2-6, z^* for cases 7-10, N_1 for cases 11-12, N_2 for cases 13-14 and m for cases 15-16.

case	γ	z^*	m	N_1	N_2 (10^{-5})
1	0.600	0.500	0.700	16.0	20.0
2	1.00	0.500	0.700	16.0	20.0
3	0.800	0.500	0.700	16.0	20.0
4	0.700	0.500	0.700	16.0	20.0
5	0.500	0.500	0.700	16.0	20.0
6	0.400	0.500	0.700	16.0	20.0
9	0.600	0.188	0.700	16.0	20.0
10	0.600	0.313	0.700	16.0	20.0
11	0.600	0.688	0.700	16.0	20.0
12	0.600	0.875	0.700	16.0	20.0
13	0.600	0.500	0.700	7.99	20.0
14	0.600	0.500	0.700	32.0	20.0
15	0.600	0.500	0.700	16.0	50.0
16	0.600	0.500	0.700	16.0	4.00
17	0.600	0.500	0.800	16.0	20.0
18	0.600	0.500	0.556	16.0	20.0

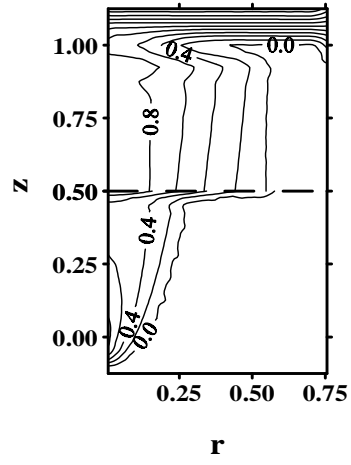
4. RESULTS

4.1 Numerical computations

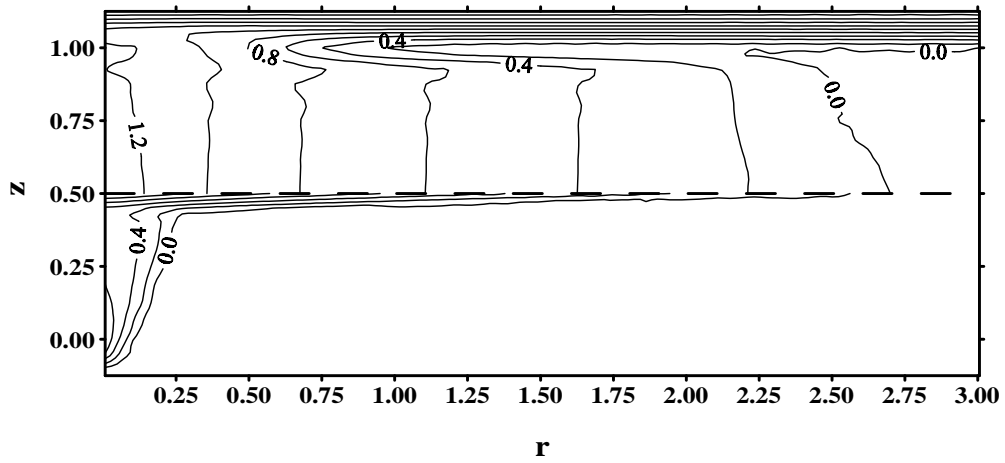
Using a numerical model [Van Dijke *et al.*, 1995] we solved the transient two-phase flow problem of Section 2 described by equations (2.1-2.6) on the finite domain $E < R < R_b$ and $-H_b < Z < H_t$ ($H_b > 0$), where R_b and H_b were chosen such that injected air never reached these boundaries. We imposed at the lower boundary a no-flow condition ($U_{j,z} = 0$). At the right boundary we imposed hydrostatic water pressures ($P_w = \rho_w g (H - Z)$), no air flow below the water table ($U_{a,r} = 0$ for $Z < H$) and hydrostatic air pressures above the water table ($P_a = \rho_a g (H_t - Z)$ for $Z > H$). The flow domain was discretized by linear triangular finite elements and time discretization was fully implicit. The resulting algebraic equations were solved by the modified Picard method, that gave good mass balances [Celia *et al.*, 1990]. In R -direction we used 30 elements of linearly increasing width (the width of the last element was 4.63 times the width of the first element). The Z -grid was uniform with 0.25 m wide elements, except for a 0.5 m thick layer from the interface downward, where we expected the vertical equilibrium regime. There, we used 5 elements of linearly decreasing thickness (the thickness of the last element was 0.220 times the thickness of the first element at the top of the layer). Convergence was obtained for the Picard iterations by adjusting the time steps. Computations were done in non-transformed physical variables.

The following soil and fluid parameters were fixed during all computations: $\phi=0.400$, $\mu_a=1.77 \cdot 10^{-5}$ Pas, $\rho_a=1.24 \text{ kg m}^{-3}$, $\mu_w=1.30 \cdot 10^{-3}$ Pas, $\rho_w=1.00 \cdot 10^3 \text{ kg m}^{-3}$, $g=9.8 \text{ m s}^{-2}$, $U_{in} = 7.07 \cdot 10^{-3} \text{ m s}^{-3}$, where the latter agrees with total injection rate of $8.00 \text{ m}^3 \text{ h}^{-1}$. Parameters involving the boundary conditions were: $E=5.00 \cdot 10^{-2} \text{ m}$, $L=1.00 \text{ m}$, $H=8.00 \text{ m}$, $H_t=9.00 \text{ m}$. We varied the exponent m , the dimensionless numbers N_1 and N_2 and the heterogeneity parameters γ and z^* with respect to the reference case (case 1) as is summarized in Table 1. Variations in N_1 and N_2 were due to variations in α^- and k^- respectively: for the reference case we used $k^- = 1.00 \cdot 10^{-10} \text{ m}^2$ and $\alpha^- = 2.00 \text{ m}^{-1}$. The values of the parameters for these simulations reflect a rather wide range of sandy soils (loamy till coarse sand).

The numerical results revealed that in every case the air flow became stationary. Defining the steady



(a)



(b)

Figure 3: Dimensionless capillary pressure contours for (a) case 1 and (b) case 2.

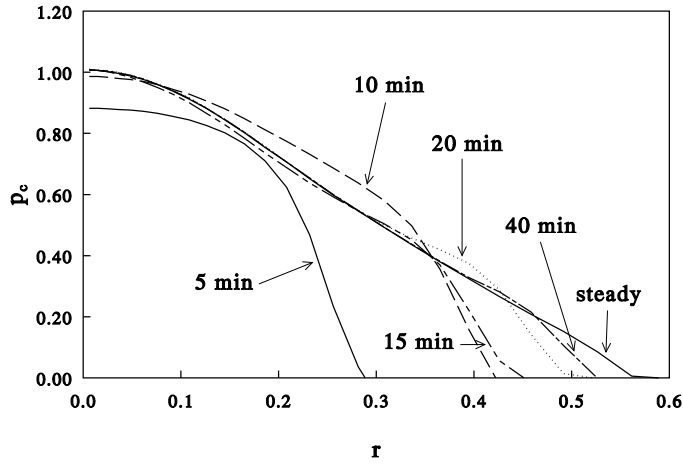


Figure 4: Dimensionless capillary pressure as a function of the radial coordinate at the interface for different times.

state time as the time whereafter the increase of air volume stored in the domain, see [Van Dijke *et al.*, 1995] is less than 1 percent, we found that this time varied between 1 and 5 h for all cases, except for case 5 (7 h), case 6 (35 h) and case 18 (25 h). The simulations required large computation times: roughly between 8 and 48 h on a HP 9000 735/125 workstation.

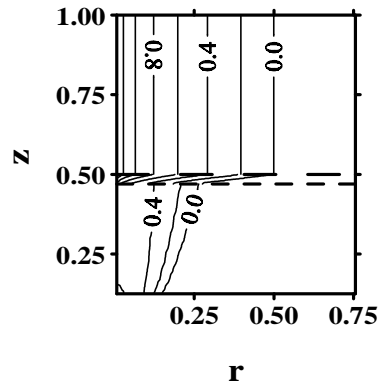
Results are presented in dimensionless form, see (2.9). We use capillary pressure (p_c) as the main variable, because it is continuous over the entire domain and has a non-zero gradient normal to the free boundary, which makes it easy to determine the position of this boundary. In Figure 3 the capillary pressure contours for case 1 and case 6 (large material contrast) at steady state are shown. These contours show a sharp transition from the buoyancy-dominated region to the vertical equilibrium region just below the interface. Furthermore, we observe that above the interface the solution is almost constant in the z -direction. As the solution at the interface is characteristic for air injection in layered media, we present in Figure 4 the development of capillary pressure at the interface towards the steady state. After injected air has reached the water table (which occurred between 10 and 15 min), air still accumulates at larger radial distances until a steady state is attained.

4.2 Applicability of the analytical approximation

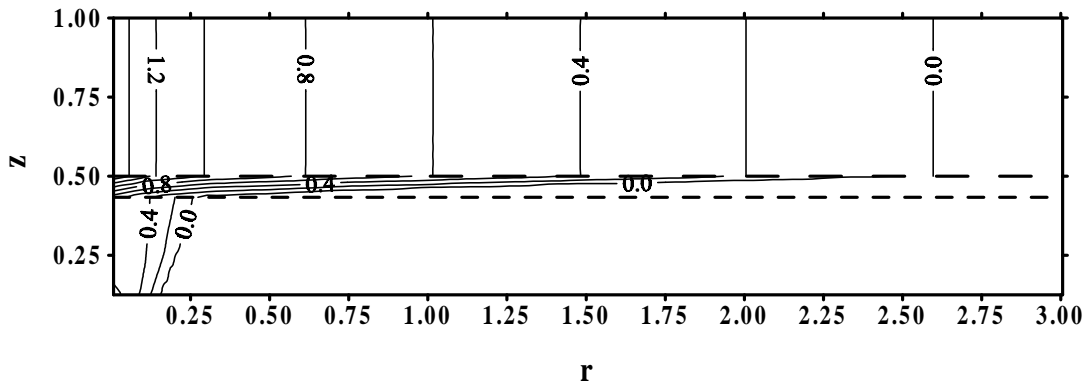
In Figure 5 we present the capillary pressure contours for case 6 as computed according to the analysis of Section 3 in regions *I*, *II* and *III*, which describe the situation between the upper part of the well screen and the water table. Comparison with Figure 3.b shows good agreement between the two solutions. In Figure 6 we show the numerical $p_n(r)$ and analytical $p_a(r)$ steady state capillary pressure functions at the interface for case 1 and 6. Observe that the agreement is much better for the larger material contrast (smaller γ) of case 6.

To quantify the agreement we compared the positions of the free boundary at the interface of the numerical f_n^+ and the analytical f_a^+ solution. Despite the fine discretization just below the interface the numerical profiles exposed small fluctuations near the free boundary. Nevertheless, we were able to accurately estimate f_n^+ from the almost constant slope of the profile at the left side of the fluctuations. In Figure 7 we present the relative errors

$$\Delta f^+ = \frac{f_n^+ - f_a^+}{f_a^+} \quad (4.1)$$

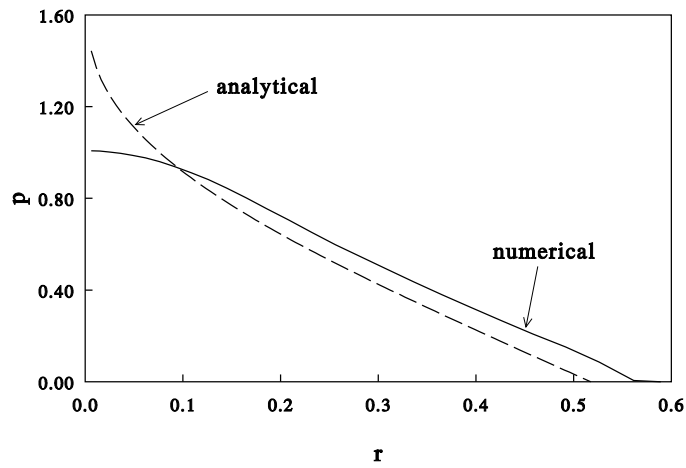


(a)

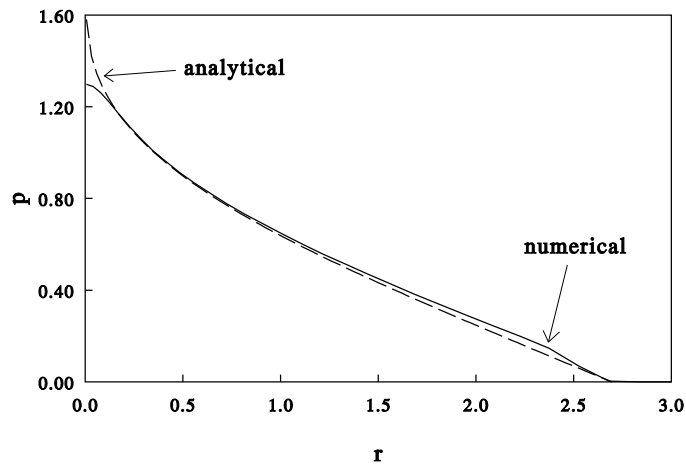


(b)

Figure 5: Analytical approximation of the dimensionless capillary pressure contours for (a) case 1 and (b) case 6.



(a)



(b)

Figure 6: Comparison of the numerically and analytically computed dimensionless capillary pressures as a function of the radial coordinate for (a) case 1 and (b) case 6 at the interface.

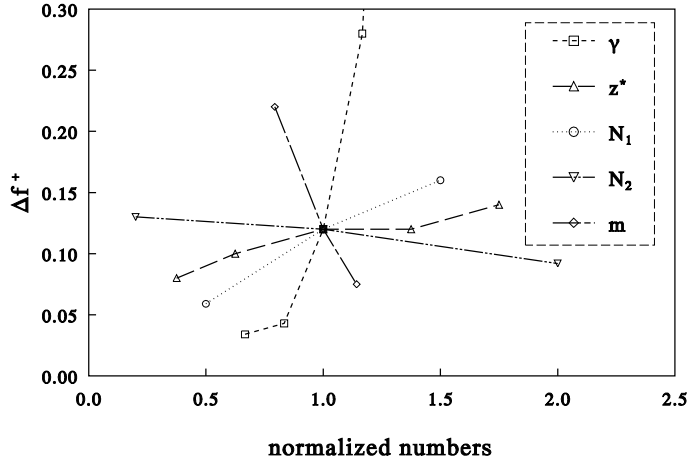


Figure 7: Relative errors Δf^+ of the position of the free boundary at the interface versus the normalized dimensionless numbers. The γ -curve reflects values of the parameters for cases 2-6, the z^* -curve for cases 7-10, the m -curve for cases 15-16, the N_1 -curve for cases 11-12 and the N_2 -curve for cases 13-14.

as functions of

$$\tilde{\gamma} = \frac{\gamma}{\gamma_r}, \quad \tilde{z}^* = \frac{z^*}{z_r^*}, \quad \tilde{m} = \frac{m}{m_r}, \quad \tilde{N}_1 = \frac{N_1}{N_{1r}}, \quad \tilde{N}_2 = \frac{N_2}{N_{2r}}, \quad (4.2)$$

which are the dimensionless numbers of Table 1 that are normalized with respect to the numbers of the reference case (subscript r). Observe that for larger values of z^* , i.e. the distance between the well and the interface, the agreement became worse, because the buoyancy-dominated solution below the interface resulted in wider air cones, that lead to larger spreading at the interface. Furthermore, we observe that the various soil and fluid parameters, which are combined in N_1 , N_2 and m , affect the error Δf^+ , but we expect that in every situation with sufficiently small γ the vertical equilibrium assumption is satisfied and that the error Δf^+ is negligible. In most practical situations the value of γ is much smaller than for the reference case ($\gamma = 0.600$) and the analytical approximation performs very well.

4.3 Sensitivity analysis

For remediation purposes mass transfer limitations to volatilization of organic contaminants and to biodegradation relate more directly to saturation than capillary pressure. Therefore, we present in Figure 8 for several values of γ , but with the other parameters as in case 1, the saturation profiles at the upper side of the interface, which are based on the analytical approximation. Because for smaller γ the profile has a very long tail with almost zero saturations, we use the first moment

$$M = \frac{\int_{\varepsilon}^{f^+} r^2 S_a(r, z^*) dr}{\int_{\varepsilon}^{f^+} r S_a(r, z^*) dr} \quad (4.3)$$

as a characteristic distance for the horizontal extension of these profiles rather than the number f^+ . M is shown in Figure 9 as a function of γ for several sets of the dimensionless numbers m , N_1 and N_2 . For small contrasts we expect that the analytical approximation is not valid. To obtain an upper bound γ_s on the values of γ for which we may apply the approximation, we computed the first moment M_s of the similarity solution (3.3) at the interface for the homogeneous situation. Hence, we define γ_s such that $M(\gamma_s) = M_s$ and we present in Figure 9 M versus γ up to this upper bound γ_s .

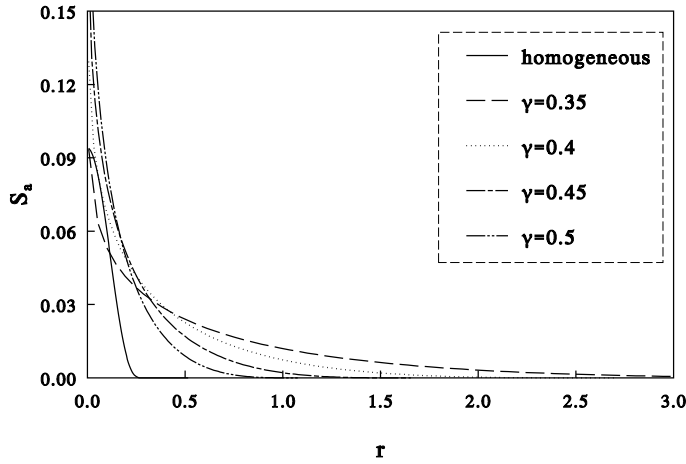


Figure 8: Analytical approximations of the saturation at the upper side of the interface as a function of the dimensionless radial coordinate for several degrees of heterogeneity.

The analysis shows that the spreading is almost insensitive to variations of N_2 , but that it varies significantly with N_1 and m . Observe that the analytical approximation does not depend on the position of the interface z^* , whereas the results of the numerical simulations reveal an effect of this parameter which diminishes for decreasing γ , as we showed earlier.

5. APPLICABILITY OF THE ANALYTICAL APPROXIMATION TO A DNAPL SPILL ABOVE A LESS PERMEABLE LAYER

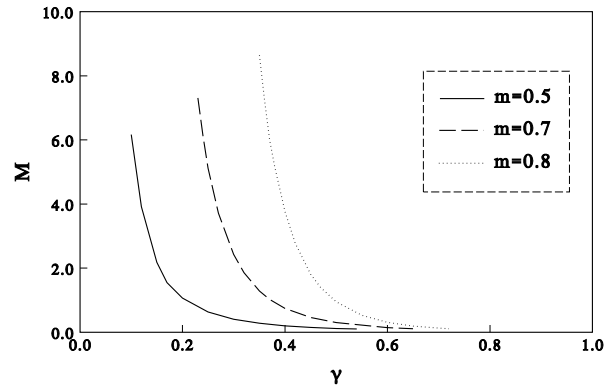
The above given analysis of air sparging in a layered soil enables us to describe also DNAPL flow below the phreatic surface towards and through a low permeable layer of large horizontal extension. DNAPL flow above a low permeable layer of finite horizontal extension was investigated by *De Neef and Molenaar* [1997]. They assumed that to enter this layer DNAPL must overcome a positive entry pressure. An analysis of the steady state situation for which all DNAPL migrates downward along the lateral boundaries of the layer, revealed the conditions under which the entry pressure is exceeded and DNAPL may infiltrate into the low permeable layer.

To show the analogy with the sparging problem, we assume that a possible entry pressure has been overcome and that at steady state all DNAPL flows through the low permeable layer. We assume that the distance between the DNAPL source and the low permeable layer is large enough for the development of a region with mainly horizontal flow in agreement with [*De Neef and Molenaar*, 1997]. Provided that the DNAPL can flow downward away from the interface, after sufficiently large time a steady state situation is reached at the interface. Hence, the steady state solution for the vertical equilibrium region provides an estimate of the maximum horizontal spreading at the interface.

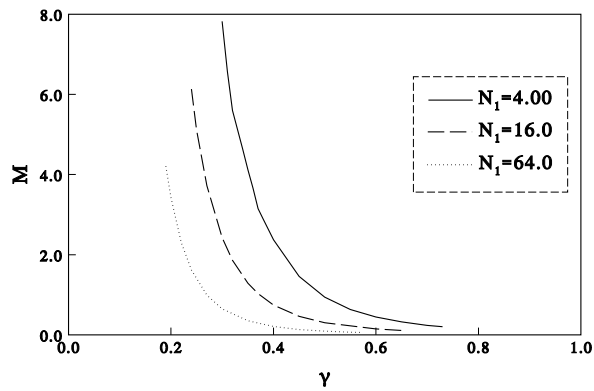
With emphasis on steady state flow above and across the interface, we outline the modifications of the air sparging analysis, that are necessary for the DNAPL flow problem. For this case, the interface Z^* of Figure 1 separates the high permeable top and low permeable bottom layers, such that (for $0 < \gamma < 1$)

$$k = \begin{cases} k^- & \text{for } Z > Z^* \\ k^+ & \text{for } Z < Z^* \end{cases} \quad \text{and} \quad \alpha = \begin{cases} \alpha^- & \text{for } Z > Z^* \\ \alpha^+ & \text{for } Z < Z^* \end{cases}, \quad (5.1)$$

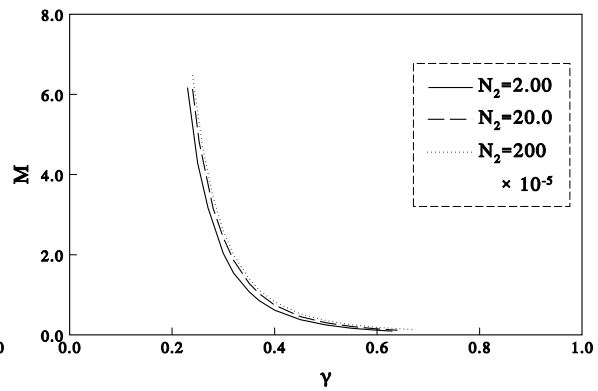
with $k^+ = \gamma^2 k^-$ and $\alpha^+ = \gamma \alpha^-$ as before. Assuming that the horizontal extension of the source and of the DNAPL flow field in the high permeable layer is small, horizontal spreading mainly occurs just



(a)



(b)



(c)

Figure 9: First moment M of the horizontal extension of the analytically approximated saturation profiles at the interface versus heterogeneity γ for several values of (a) m , (b) N_1 and (c) N_2 .

above the interface. For convenience we still consider a domain with $R > E$ to avoid singularities at $R = 0$.

Equations (2.1) and (2.2) are used with the subscript a for air replaced by o for oil (DNAPL). Because in this steady state situation the water velocity is not negligible due to the smaller difference in density and viscosity [De Neef and Molenaar, 1997], we use instead of equation (2.8), the fractional flow formulation for the oil velocity, see e.g. [Bear, 1972; Chavent and Jaffr e, 1986],

$$\vec{U}_o = F_o \vec{U}_t - \frac{k k_{rw}}{\mu_w} F_o \nabla (P_c - \Delta \rho g Z), \quad (5.2)$$

where the oil fractional flow function F_o and the mobility ratio M are defined by

$$F_o = \frac{k_{ro}}{k_{ro} + M k_{rw}} \quad \text{and} \quad M = \frac{\mu_o}{\mu_w}, \quad (5.3)$$

the total flow velocity $\vec{U}_t = \vec{U}_w + \vec{U}_o$ and $\Delta \rho = \rho_o - \rho_w$. We introduce dimensionless variables according to (2.9) and (2.10), where H is redefined as the distance between the well and the interface. Hence, we obtain in dimensionless form

$$\nabla \cdot \vec{u}_o = 0, \quad (5.4)$$

and

$$\vec{u}_o = \begin{cases} F_o \vec{u}_t - M k_{rw} F_o (N_c \nabla p_c - N_g \vec{e}_z) & \text{for } z > z^* \\ F_o \vec{u}_t - M k_{rw} F_o (\gamma N_c \nabla p_c - \gamma^2 N_g \vec{e}_z) & \text{for } z < z^*, \end{cases} \quad (5.5)$$

with the obvious substitution of the newly defined $\Delta \rho$ in N_g , N_1 and N_2 .

Using similar assumptions as in equations (3.6-3.8) we arrive at the vertical equilibrium assumption

$$\frac{\partial p_c}{\partial z} \sim -\frac{N_g}{N_c} \quad (5.6)$$

for the entire region of thickness $z_f - z^*$ on top of the low permeable layer. If oil saturations are small, we may assume that the total velocity $\vec{u}_t = 0$, i.e. counter-current flow $\vec{u}_w = -\vec{u}_o$ [De Neef and Molenaar, 1997]. Following the derivation of Section 3 we obtain the boundary value problem for the pressure at the interface $p(r)$:

$$\begin{cases} \frac{d}{dr} (r \tilde{D}(p) \frac{dp}{dr}) - r \gamma^2 N_1^2 \lambda(\gamma p) = 0 & \text{for } \varepsilon < r < f^+ \\ -(r \tilde{D}(p) \frac{dp}{dr})|_{r=\varepsilon} = \frac{N_1^2 N_2}{2}, \quad p(f^+) = 0, \end{cases} \quad (5.7)$$

where $\tilde{D} = \int_0^p \lambda(\xi) d\xi$, with $\lambda(p_c) = M k_{rw}(S_o(p_c)) F_o(S_o(p_c))$. However, as p and S_o are small, the water mobility k_{rw}/μ_w is much larger than the oil mobility k_{ro}/μ_o and as a result the function $\lambda(p)$ is approximately equal to $\kappa(p)$. Hence, the boundary condition

$$\frac{dp}{dr}(f^+) = -\gamma^{1+\frac{1}{2pD}} N_1 \quad (5.8)$$

is also valid for problem (5.7). Furthermore, we conclude that for small p and S_o problem (3.17) is a good approximation of problem (5.7).

The number f^+ provides an estimate of the maximum spreading radius of DNAPL on top of the low permeable layer.

To illustrate the analogy between the sparging and the DNAPL problems, we additionally carried out a simulation for DNAPL infiltration. In an axisymmetric domain with $0.05 \leq R \leq 10.05$ m and

$0.0 \leq Z \leq 8.0$ m the interface between the high permeable top and the low permeable bottom layer was positioned at $Z = 4.0$ m. DNAPL infiltrated at the top through a horizontal source with outer radius 0.557 m at velocity $2.87 \cdot 10^{-4}$ m s $^{-1}$, which yields a total rate of 1.0 m 3 h $^{-1}$.

Initially water pressures were hydrostatic, such that the water table was positioned at $Z = 10$ m and no DNAPL was present in the domain. The top, left and bottom boundary were impermeable to water, whereas at the right boundary the initial pressure distribution was imposed. The top boundary (except for the source) and the left and right boundary were impermeable to oil, whereas at the bottom boundary oil pressure heads were fixed at 10.0 m, i.e. equal to the initial water pressure heads. These boundary conditions allowed water flow through the right boundary and oil outflow through the bottom boundary. Although the configuration was slightly different from the sparging situation, we assumed that the differences did not affect the flow in the neighbourhood of the interface.

We imposed a heterogeneity of $\gamma = 0.60$, whereas $H = 4.0$ m. For DNAPL we took $\rho_o = 1.50$ m 3 kg m $^{-3}$ and $\mu_o = 0.65 \cdot 10^{-3}$ Pa s. All other parameters were taken as in case 1 for the sparging problem. Consequently, we had $z^* = 1.0$, $m = 0.700$, $N_1 = 4.0$ and $N_2 = 7.33 \cdot 10^{-3}$.

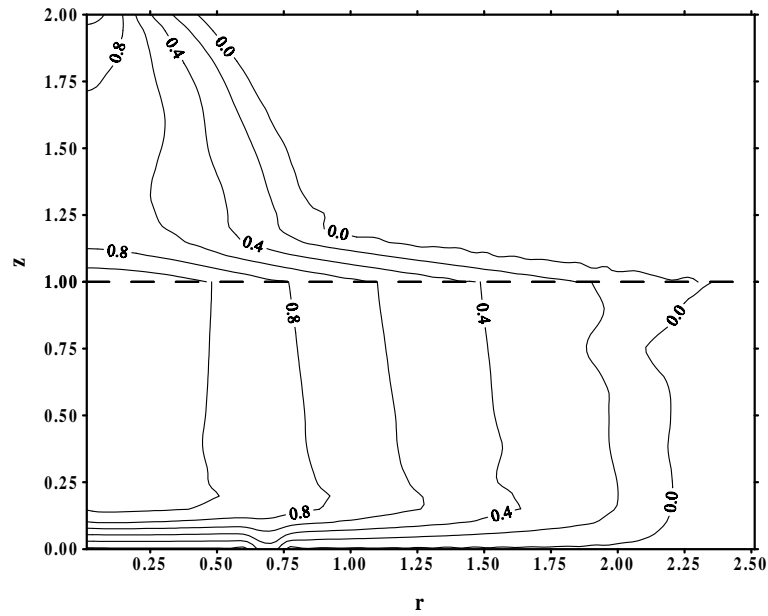
This simulation led also to a steady state situation with DNAPL flowing mainly horizontally on top of the interface. Compared to the sparging situation the time necessary to reach steady state was much larger (i.e. about 85 h). At steady state the water pressure distributions were approximately hydrostatic. In Figure 10 we present the steady state capillary pressure contours, which have essentially the same pattern as the contours for the sparging situation with the same heterogeneity of Figure 3.a. Comparison shows that in spite of the lower injection rate capillary pressures and radial extension are larger for DNAPL than for air.

In view of the hydrostatic water pressures we approximated λ by κ in problem (5.7). We solved this problem for the capillary pressures at the interface and compared the solution with the numerical solution in Figure 10.b. The agreement between the two curves is as least as good as in Figure 5.a, which is understandable in view of the larger radial spreading. Hence, the analytical approximation is also useful to describe DNAPL flow over a low permeable layer and the agreement will strongly increase when heterogeneity is increased. Since DNAPL flow proceeds much slower than air flow, the steady state may not always be reached within realistic times. Still, the analytical approximation provides a good estimate of the maximum radial extension of DNAPL flow in a layered soil.

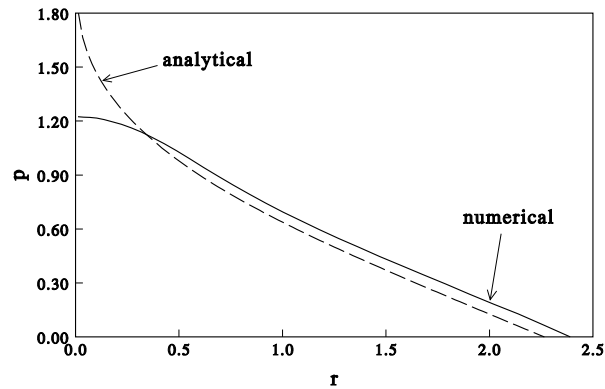
6. CONCLUSIONS

We modeled air sparging into an aquifer below a less permeable horizontal layer as multi-phase flow of two immiscible fluids. The two layers were assumed to have similar structure but different mean pore size.

We found that flow approaches a steady state, that is characterized by three dimensionless numbers which also control the flow problem for a homogeneous domain and by two numbers which correspond to the position of the interface between the two layers and to the degree of material contrast respectively. Analyzing the steady state situation we distinguished three regions with different flow regimes. In the lower layer above the well screen the vertical flow component is dominated by buoyancy-induced forces. Just below the interface a regime with almost vertical flow equilibrium conditions develops, where air tends to spread mainly horizontally. Above the interface the vertical flow component is buoyancy-dominated. In the lowest region steady state flow is approximated by a similarity solution that applies in homogeneous situations [Van Dijke et al., 1995]. We analyzed the region just below the interface separately from the lowest region, but incorporated continuity of pressure and vertical flow velocity at the interface towards the less permeable region. Assuming hydrostatic pressures we derived a diffusion equation for the capillary pressure at the interface with a 'loss term' corresponding to the flow through the interface. With a simple numerical procedure we obtained the solution of this ordinary differential equation, which is non-zero within a finite interval of the radial coordinate. This solution determines the capillary pressures in the region below the interface and the free boundary enclosing this region, beyond which air is absent. Between the interface and the water table we assumed that no further changes occur in the radial direction compared to the solution at the interface.



(a)



(b)

Figure 10: DNAPL infiltration in a high permeable layer on top of a low permeable layer with a heterogeneity $\gamma = 0.60$: (a) dimensionless capillary pressure contours and (b) comparison of the numerically and analytically computed dimensionless capillary pressures as a function of the radial distance at the interface.

Using a numerical two-phase flow model we made transient computations for several values of the dimensionless numbers. These computations were very time consuming. In every case we found that the flow reached a steady state situation. However, the time that this was the case and the horizontal spreading of air below the interface increased much with increasing heterogeneity and with increasing values of the exponent m . Only for almost homogeneous flow domains, the position of the interface relative to the well screen affected the steady state air flow significantly.

We compared the numerical and analytical approximations of the steady state situation with emphasis to the solution at the interface. The agreement between the numerically and analytically obtained radii of influence at the interface was very good when these radii were large compared to the radii of the corresponding homogeneous situations. Else, the vertical equilibrium assumption was less satisfied or the flow below the region with vertical equilibrium affected the numerical solution at the interface significantly.

Because from the remediation point of view the saturation is one of the most important variables, we considered the analytically obtained saturation profile at the interface. We observed that for large values of the radii of influence saturations are almost zero in a large part of the profile. Therefore, we carried out an analysis of the relation between the degree of heterogeneity and the first moment of the horizontal extension of the saturation profile at the interface for several values of the remaining dimensionless parameters. As was expected this spatial moment increases much with increasing heterogeneity and is most sensitive to variations in the exponent m and the dimensionless number N_1 .

With minor modifications the present analysis enables also the description of the maximum radius of horizontal spreading in case of DNAPL flow over a low permeable layer. We showed by a representative numerical simulation that the time necessary to reach steady state for DNAPL infiltration is much larger than for air sparging. Furthermore, the radial spreading at the interface is larger and as a result the agreement between numerical and analytical approximations is at least as good as in the sparging situation.

APPENDIX 1: EVALUATION OF THE BOUNDARY VALUE PROBLEM

For steady state flow the free boundary $z_f(r)$ is tangential to the air flow direction. This yields at $r = f^+$

$$\frac{dz_f}{dr}\Big|_{r=f^+} = \lim_{r \rightarrow f^+} \frac{u_{a,z}(r, z^*)}{u_{a,r}(r, z^*)} = \lim_{r \rightarrow f^+} \frac{\gamma^2 N_g \kappa(\gamma p(r))}{-N_c \kappa(p(r)) \frac{dp}{dr}(r)}, \quad (\text{A } 1)$$

where we have used the righthandside of relation (3.6) for $u_{a,z}(r, z^*)$. We differentiate equation (3.11) with respect to r and use it in relation (A 1), which yields

$$\lim_{r \rightarrow f^+} \left(\frac{dp}{dr}(r, z^*) \right)^2 = \lim_{r \rightarrow f^+} \gamma^2 N_1^2 \frac{\kappa(\gamma p(r))}{\kappa(p(r))}. \quad (\text{A } 2)$$

Using the power law approximation for $\kappa(p)$ (3.1), which is exact if k and p approach zero, we obtain condition (3.18). Setting $q = p'$, where primes ' denote differentiation with respect to r , we transform problem (3.17) into the system of first order equations

$$\begin{cases} p' &= q \\ q' &= -\frac{q}{r} - \kappa(p) \frac{q^2}{D(p)} + \lambda_1 \frac{\kappa(\gamma p)}{D(p)}, \end{cases} \quad (\text{A } 3)$$

for $r \in (\varepsilon, f^+)$, with boundary conditions

$$(r D(p) q)|_{r=\varepsilon} = -\lambda_2, \quad p(f^+) = 0, \quad q(f^+) = -\lambda_3, \quad (\text{A } 4)$$

where

$$\lambda_1 = \gamma^2 N_1^2, \quad \lambda_2 = \frac{N_1^2 N_2}{2}, \quad \lambda_3 = \gamma^{1+\frac{1}{2pD}} N_1. \quad (\text{A } 5)$$

Using again the power law approximation for $\kappa(p)$ in system (A 3), we obtain additionally $q'(f^+) = \frac{\lambda_3}{f^+} \frac{p_D}{3p_D + 2}$, with p_D given by (3.2). Hence, we use a fourth order Runge-Kutta routine to integrate (A 3) iteratively from $r = f^+$ to $r = \varepsilon$, while varying f^+ until the condition at $r = \varepsilon$ is matched.

ACKNOWLEDGEMENT

This project was partly funded by the Netherlands Organization for Scientific Research (NWO project NLS 61-251), and carried out with the use of computing facilities of the Department of Mathematics of Delft University of Technology.

REFERENCES

- Barenblatt, G.I., On some unsteady motions of a liquid or a gas in a porous medium, *Prikl. Mat. Mekh.*, 16, 67-78, 1952 (in Russian).
- Bear, J., *Dynamics of fluids in porous media*, Elsevier, New York, 1972.
- Celia, M.A., E.T. Bouloutas and R.L. Zarba, A general mass-conservative numerical solution for the unsaturated flow equation, *Water Resour. Res.*, 26, 1483-1496, 1990.
- Chavent, G. and J. Jaffré, Mathematical models and finite elements for reservoir simulation, in *Studies in mathematics and its applications*, vol. 17, edited by J.L. Lions e.a., North-Holland, Amsterdam, 1986.
- De Neef, M.J. and J. Molenaar, Analysis of DNAPL infiltration in a medium with a low permeable lens, *Comp. Geosciences*, 1, 191-214, 1997.
- Ji, W., A. Dahmani, D.P. Ahlfeld, J.D. Lin and E.H. Hill III, Laboratory study of air sparging: air flow visualization, *Ground Water Mon. Rev.*, 13, 115-126, Fall 1993.
- Johnson R.L., P.C. Johnson P.C, D.B. McWorther, R.E. Hinchee and I. Goodman, An overview of in situ air sparging, *Ground Water Mon. Rev.*, 13, 127-135, Fall 1993.
- Leverett, M.C., Capillary behaviour in porous solids, *Trans. Am. Inst. Min. Metall. Pet. Eng.*, 142, 152-169, 1941.
- Lundegard, P.D., and D. LaBrecque, D., Air sparging in a sandy aquifer (Florence, Oregon, USA): Actual and apparent radius of influence, *J. Contam. Hydrol.*, 19, 1-27, 1995.
- Marley, M.C., D.J. Hazebrouch, and M.T. Walsh, The application of in situ air sparging as an innovative soils and ground water remediation technology, *Ground Water Mon. Rev.*, 12, 137-145, Spring 1992.
- McCray, J.E. and R.W. Falta, Defining the air sparging radius of influence for groundwater remediation, *J. Contam. Hydrol.*, 24, 25-52, 1996.
- Miller, E.E., Similitude and scaling of soil-water phenomena, in *Applications of soil physics*, edited by D. Hillel, Academic Press, New York, 1980.
- Mohtar, R.H., R.B. Wallace and L.J. Segerlind, Finite element simulation of oil spill cleanup using air sparging, in *Computational methods in water resources X, Vol. 2*, edited by A. Peters e.a., pp. 967-974, Kluwer Academic Publishers, Dordrecht, 1994.
- Parker, J.C., R.J. Lenhard, and T. Kuppusamy, A parametric model for constitutive properties governing multiphase flow in porous media, *Water Resour. Res.*, 23, 618-624, 1987.

- Pattle, R.E., Diffusion from an instantaneous point source with a concentration-dependent coefficient, *Quart. J. Mech. Appl. Math.*, *12*, 407-409, 1959.
- Unger, A.J.A., E.A. Sudicky and P.A. Forsyth, Mechanisms controlling vacuum extraction coupled with air sparging for remediation of heterogeneous formations contaminated by dense nonaqueous phase liquids, *Water Resour. Res.*, *31*, 1913-1925, 1995.
- Van Dijke, M.I.J., C.J. van Duijn and S.E.A.T.M. van der Zee, Multi-phase flow modeling of air sparging, *Adv. Water Resour.*, *18*, 319-333, 1995.
- Wehrle, K., In-situ cleaning of CHC contaminated sites: model-scale experiments using the air injection (in-situ stripping) method in granular soils, in *Contaminated soil '90*, edited by F. Ahrendt e.a., pp. 1061-1062, Kluwer Academic Publishers, Dordrecht, 1990.